Nanoscale

ROYAL SOCIETY OF CHEMISTRY

PAPER

View Article Online
View Journal | View Issue

Cite this: *Nanoscale*, 2024, **16**, 21545

Stimuli-responsive anion transport utilising caged hydrazone-based anionophores†

Manzoor Ahmad, Martin Flerin, Hui Min Tay, Amber L. Thompson,
Fernanda Duarte* and Matthew J. Langton*

Received 5th August 2024,
Accepted 28th October 2024

DOI: 10.1039/d4nr03220a

rsc.li/nanoscale

Ion transport across biological membranes, facilitated by naturally occurring ion channels and pumps, plays a crucial role in biological processes. Gating is an important aspect of these systems, whereby transport is regulated by a range of external stimuli such as light, ligands and membrane potential. While synthetic ion transport systems, especially those with gating mechanisms, are rare, they have garnered significant attention due to their potential applications in targeted therapeutics as anticancer agents or to treat channelopathies. In this work, we report stimuli-responsive anion transporters based on dynamic hydrogen bonding interactions of hydroxyl-functionalised hydrazone anionophores. Caging of the hydroxyl groups with moities that are responsive to light and H_2S locks the hydrazone protons through intramolecular hydrogen bonding, rendering them unavailable for anion binding and transport. Upon decaging with light or H_2S, the hydrogen bonding pattern is reversed, rendering the hydrazone protons available for anion binding, and leading to efficient switch-on of ion transport across the lipid bilayer membrane.

I. Introduction

Gating of biological ion transport proteins regulates their activity, and is triggered by a wide range of stimuli, including light, membrane potential, and small molecule ligand binding.[1–3] Malfunctioning ion transport proteins cause a variety of diseases, collectively called 'channelopathies'.[4–6] Synthetic transport systems have emerged as an important class of compounds that have potential as chemotherapeutics to treat channelopathies, particularly in the context of chloride anionophores for cystic fibrosis, or *via* exploiting ion transport-triggered apoptosis for cancer therapy.[7–10] Stimuli-responsive systems in particular are of significant interest for spatiotemporally controlled activation in targeted therapeutics. To achieve this, various stimuli including pH, light, enzymes, redox and voltage have been employed.[11–21] Reversibly gated systems that commonly exploit photoisomerization of azobenzene[22–26] and stilbene[27] often exhibit background transport activity because of incomplete photoconversion or suffer from fast thermal relaxation which limits their applicability in biological contexts. In contrast, irreversibly controlled transporters that are triggered by decaging reactions enable very effective off-on control over transport, and overcome the challenges of incomplete activation or deactivation in photo-switchable systems. Examples include the use of photo-responsive cages to block the anion binding sites in anion carriers,[28,29] modulate the self-assembly pattern of channel forming monomers,[30] or control the mobility of anionophores.[31]

Recently, a new approach has been developed in which dynamic hydrogen bonding interactions were employed to generate responsive ion transport systems. Ren and coworkers reported non-covalently stapled self-assembled H^+/Cl^- channels utilizing photo-decaging of alkyl-functionalized dihydroxy isophthalamide derivatives.[32] We have demonstrated that a similar concept could be utilized for accessing multiple stimuli-responsive moieties, in which light, redox or enzymatic decaging of pro-carriers leads to a intramolecular hydrogen bonding switch, and activation of ion transport, including with dual-caged AND logic activation.[33]

Here, we demonstrate that efficient off-on activation of transport, with negligible background activity in the off state and high transport activities in the on state, can be achieved using stimuli-triggered decaging of hydrazone based anionophores that operate *via* an intramolecular hydrogen bond switch. We show that this system can be readily modified, to access transporters efficiently activated using light or H_2S as a biologically relevant redox stimulus.

II. Results and discussion

Approach

We envisaged that replacing the amide motif in our previously reported system with an acyl hydrazone anion binding motif

---

*Chemistry Research Laboratory, Mansfield Road, Oxford, OX1 3TA, UK.
E-mail: matthew.langton@chem.ox.ac.uk*

† Electronic supplementary information (ESI) available. CCDC 2371936 and 2371937. For ESI and crystallographic data in CIF or other electronic format see DOI: **https://doi.org/10.1039/d4nr03220a**

would enhance the anion binding as it provides a binding core with multiple hydrazone N–H and imine–N–C–H hydrogen bonding interactions, and enhanced ion transport activity. Accordingly, we designed 4,6-dihydroxyisophthalohydrazone-derived transporters to develop dynamic hydrogen bonding-based responsive anionophores that are activated by either light or H_2S (Fig. 1). In this design, dual-caging of the hydroxy groups with *ortho*-nitrobenzyl (*ONB*) and azido cages locks the anion binding hydrazone protons through intra-molecular hydrogen bonding, inhibiting anion binding and hence anion transport. Decaging of both hydroxy groups, using light or H_2S respectively, reverses the hydrogen bonding pattern such that the hydrazone N*H* protons are available for anion binding and transport (Fig. 1C). A library of four different transporters **1–4** containing variable aromatic moieties were designed and synthesized, varying the nature of the aromatic groups to tune lipophilicity, and optimise the permeability and transport affinity of these anionophores (Fig. 1B).

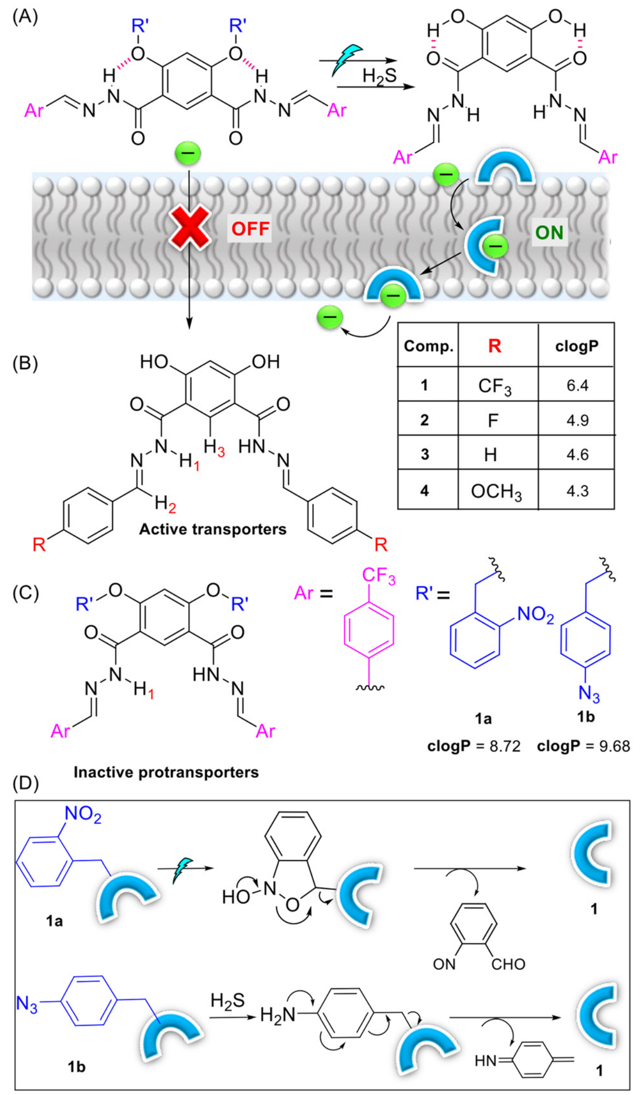

Comp.	R	clogP
1	CF_3	6.4
2	F	4.9
3	H	4.6
4	OCH_3	4.3

Fig. 1 (A) Schematic representation of stimuli-responsive anion transport. (B) Chemical structure of active transporters **1–4** and (C) caged protransporters. (D) Activation mechanisms with light and H_2S.

Synthesis and binding of active transporters 1–4

The synthesis of anion transporters **1–4** was achieved by reacting compound **5** with hydrazine hydrate to form compound **6**, which upon coupling with different aromatic aldehydes **7a–7d** yielded acylhydrazones **1–4** in excellent yield (Fig. 2A). Full experimental details and characterisation are available in the ESI.† Subsequently, chloride anion binding studies were initially carried out by ^1H NMR titration experiments. Titration of **1–4** with tetrabutylammonium chloride (TBACl) in DMSO-d_6 led to changes in H_1, H_2, and H_3 protons, revealing their role in chloride binding through hydrazone-N–$H_1\cdots Cl^-$, imine–C–$H_2\cdots Cl^-$, and ArC–$H_3\cdots Cl^-$ hydrogen bonding interactions (Fig. 2B, S34, S36, S38, and S40†). The data could be fitted to a 1 : 1 binding isotherm using Bindfit, to afford association constants values ($K_{a(1:1)}/Cl^-$) of 168 M^{-1} ± 4% for **1**, 165 M^{-1} ± 4% for **2**, 150 M^{-1} ± 4% for **3**, and 167 M^{-1} ± 3% for **4**, respectively (Fig. 2C, S35, S37, S39, and S41†). Moreover, we also performed the chloride binding analysis of the previously reported amide-based transporter **5′** in DMSO-d_6 for means of comparison.[33] Importantly, compound **5′** displayed very weak binding in the solution phase compared to the hydrazone derivatives (($K_{a(1:1)}$/Cl^-) of 64 M^{-1} ± 1%) demonstrating that replacing amide with hydrazone motifs significantly enhances the anion binding, which in turn should improve the ion transport activity (Fig. 2E, S42 and S43†).

Crystallographic studies of 1 with TBACl

Further evidence for the binding mode of chloride within the isophthalohydrazone binding cavity was obtained by single crystal X-ray diffraction studies. Crystals of **1** with Cl^- were obtained by mixing **1** and tetrabutylammonium chloride (TBACl) in dimethyl sulfoxide in 1 : 5 ratio. Slow evaporation led to the formation of colourless needle-like crystals. The structure reveals the complementarity of the binding cavity for the chloride anion, which interacts with the receptor molecule through convergent amide–N–$H_1\cdots Cl^-$, imine–C–$H_2\cdots Cl^-$, and ArC–$H_3\cdots Cl^-$ hydrogen bonding interactions, in agreement with the change of chemical shift value of these protons observed in ^1H NMR binding studies (Fig. 3). Furthermore, both NMR and crystallographic studies revealed a 1 : 1 receptor : Cl^- binding stoichiometry.

Ion transport studies

Having confirmed that compounds **1–4** were effective chloride receptors in the solution phase, ion transport experiments in large unilamellar vesicles (LUVs) encapsulating the chloride sensitive fluorophore lucigenin were performed. LUVs were prepared by entrapping lucigenin (1 mM) and sodium nitrate (200 mM) buffered at pH of 6.5 using the phosphate buffer (10 mM). Ion transport was monitored by creating a 33.3 mM Cl^- gradient across the membrane by adding sodium chloride as a pulse (50 μL, 2.0 M) in the extravesicular buffer. The rate of fluorescence quenching for lucigenin was recorded upon

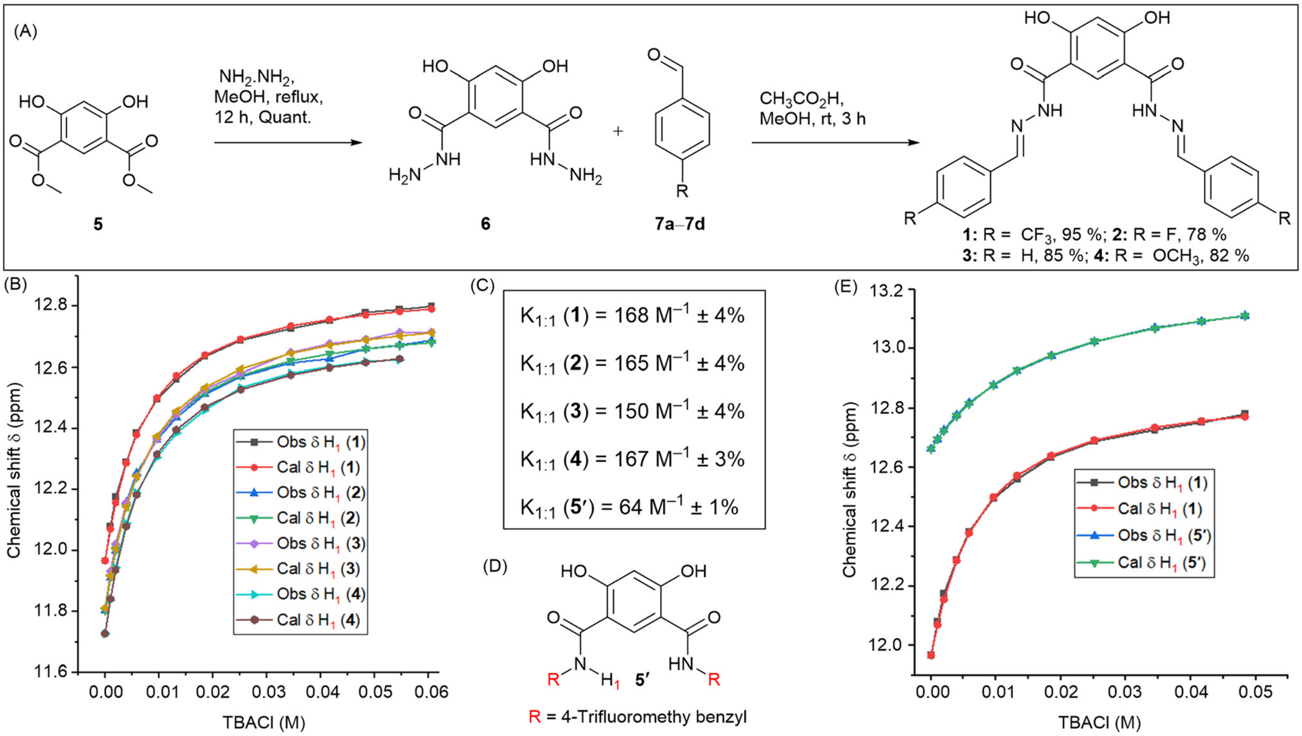

Fig. 2 (A) Chemical synthesis of active transporters **1–4**. (B) The plot of chemical shift (*δ*) of H1 proton *vs.* concentration of TBACl added, fitted to 1 : 1 binding model of BindFit v0.5 for the active transporters **1–4**. (C) Binding constant values of transporters **1–4**. (D) Chemical structure of amide-based transporter **5′**. (E) The plot of chemical shift (*δ*) of H1 proton *vs.* concentration of TBACl added, fitted to 1 : 1 binding model of BindFit v0.5 for hydrazone-based transporters **1** and amide-based transporter **5′**.

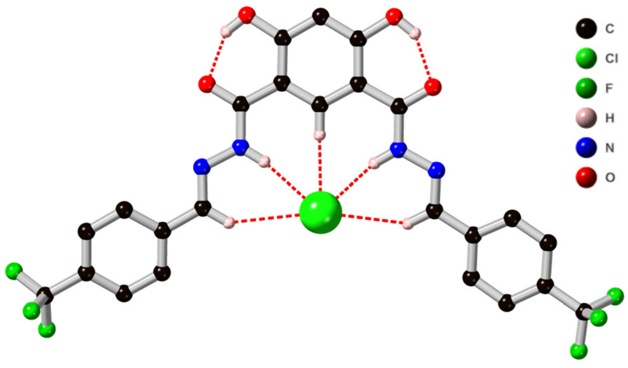

Fig. 3 Molecular structure of **1** with chloride anion from single crystal X-ray diffraction studies. The tetrabutylammonium (TBA) cation, selected hydrogen atoms and minor components of disorder are omitted for clarity.

the addition of transporters **1–4** and **5′**. These experiments revealed an activity sequence for the transport of **1** > **2** > **3** > **5′**> **4**, determined by monitoring the chloride transport at a loading of 0.055 mol% with respect to lipid (Fig. 4A). Dose–response curves for each transporter revealed the EC_{50} values of 0.035 ± 0.002 mol% for **1**, 0.042 ± 0.002 mol% for **2**, and 0.063 ± 0.002 mol% for **3**, respectively (Table 1, Fig. S49–S51†). Hill analysis could not be performed for transporter **4** due to precipitation issues at higher concentration (Fig. S52†). The above activity sequences of **1** > **2** > **3** > **4** is most likely determined by variation in the lipophilicities of the transporters, given the similarities of the chloride binding constants across the series, with most active transporter **1** having optimum clog*P* value. Notably, the hydrazone transporter **1** showed almost three-fold enhancement in the ion transport activity compared to the amide-based transporter **5′** that was used in the previous studies. This result is likely the outcome of the enhanced anion binding affinity. Hill coefficients of ∼2 is indicative of two molecules of the carrier binding to the anion to facilitate transport.

Mechanistically, chloride transport in the above studies could in principle occur either through M^+/Cl^- symport, Cl^-/NO_3^- antiport, or H^+/Cl^- symport pathways. Variation of the cations in the external buffer using different MCl solutions (M^+ = Li^+, Na^+, K^+, Rb^+, Cs^+) did not affect the ion transport activity, ruling out the possible M^+/Cl^- symport pathway for chloride transport (Fig. 4C). To distinguish between the possible Cl^-/NO_3^- antiport and H^+/Cl^- symport pathways, we performed a variation on the lucigenin assay, in which lucigenin was encapsulated inside the vesicles in the presence of NaCl (200 mM). The change in lucigenin fluorescence was monitored in the presence of **1** following addition of either Na_2SO_4 or $NaNO_3$ salt solutions in the external buffer. Significant transport was observed only in the presence of nitrate, which suggests that a Cl^-/NO_3^- antiport pathway dominates in this

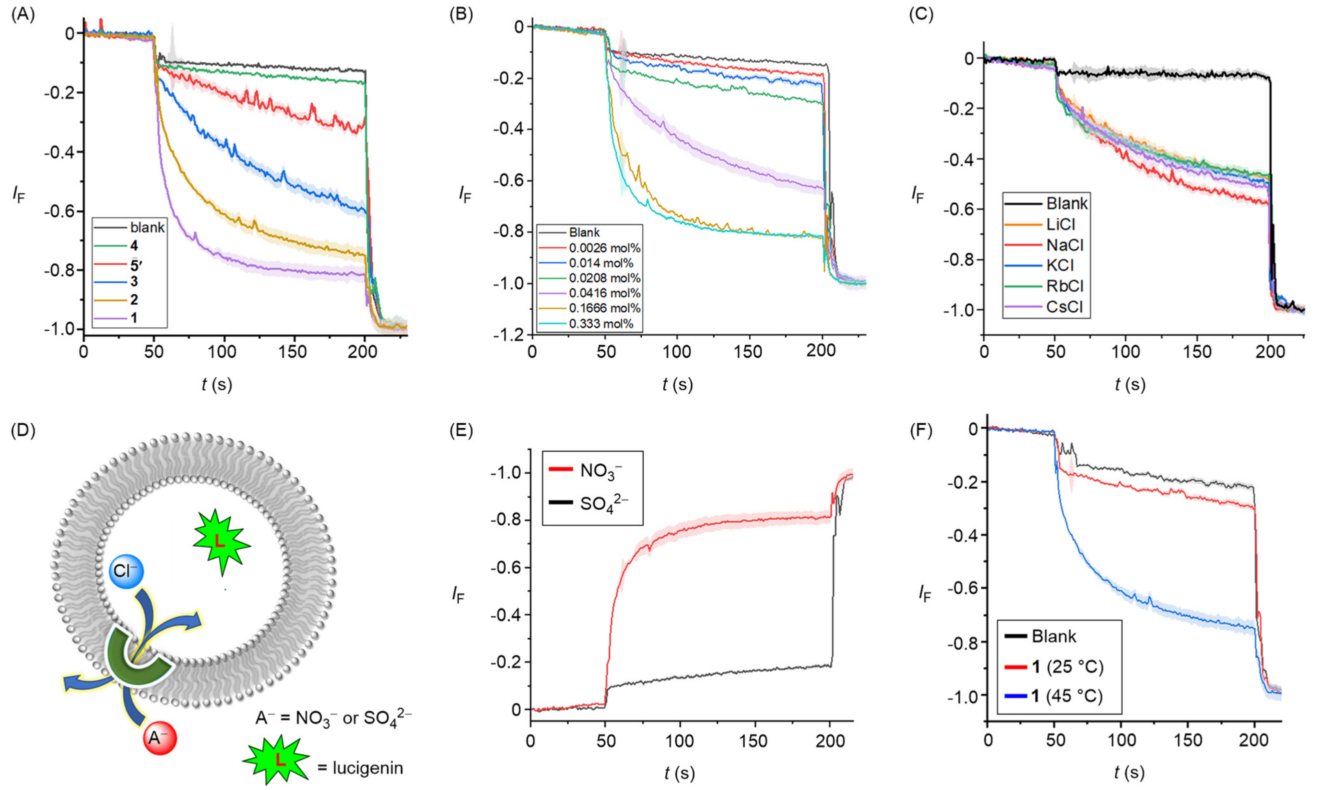

Fig. 4 (A) Activity comparison of **1–5** (0.30 mol%) across POPC-LUVs ⊃ lucigenin. (B) Concentration dependent activity of **1** across POPC-LUVs ⊃ lucigenin. (C) Cation selectivity of **1** (0.035 mol%) by varying the external cations using different MCl external buffers (M^+ = Li^+, Na^+, K^+, Rb^+, Cs^+). (D) Schematic representation of lucigenin-based chloride efflux using either extravesicular SO_4^{2-} or NO^{3-} ions. (E) Ion transport activity of **1** (0.3 mol%) in presence of external SO_4^{2-} and NO^{3-} ions. (F) Ion transport activity of **1** (0.30 mol%) across DPPC-based vesicles at 25 °C and 45 °C temperatures, respectively.

Table 1 Summary of clog P, chloride binding K_a (M^{-1}), EC_{50} (mM), and Hill coefficient (n) values

Comp.	clog P	K_a [a] (M^{-1})/Cl^-	EC_{50} [b] (mol%)	n [c]
1	6.4	168 M^{-1} ± 4%	0.035 ± 0.0016	2.4 ± 0.21
2	4.9	165 M^{-1} ± 4%	0.042 ± 0.0022	2.5 ± 0.34
3	4.6	150 M^{-1} ± 4%	0.063 ± 0.0022	2.5 ± 0.24
4	4.3	167 M^{-1} ± 3%	>0.5[d]	—[d]
5′	6.0	64 M^{-1} ± 1%	0.092 ± 0.0012	1.8 ± 0.02

[a] Association constants were obtained using the BindFit Program based on the 1 : 1 binding model for NH_1 proton. [b] Effective concentration to reach 50% of maximal activity across POPC-LUVs entrapped with 1 mM lucigenin, $NaNO_3$ (200 mM), buffered at pH 6.5 using 10 mM phosphate buffer. [c] Hill coefficient. clog P values were calculated using MarvinSketch software. [d] EC_{50} could not be reliably determined due to precipitation at higher concentrations.

assay (Fig. 4E). For Cl^-/X^- antiport, NO_3^- or SO_4^{2-} co-transport is requisite for chloride efflux, the latter being too hydrophilic to be readily transported. Conducting analogous experiments in dipalmitoylphosphatidylcholine (DPPC) LUVs provided evidence for a mobile carrier mechanism. Inactivity at 25 °C, and restoration of activity at 45 °C which is above the gel– liquid phase transition temperature for DPPC (T_m = 41 °C), is indicative of a mobile carrier process, rather than transport mediated by self-assembly into an ion channel, that activity of which would be typically expected to be invariant to lipid phase (Fig. 4F).

Synthesis and binding studies of protransporters 1a and 1b

Having demonstrated that compound **1** displayed the maximum ion transport activity, we selected this anionophore as the core scaffold for caging with stimulus-responsive groups (Fig. 5). In order to synthesize the *ONB*-based protransporter **1a**, 4,6-dihydroxyisophthalate **5** was reacted with 1-(bromomethyl)-2-nitrobenzene **8** to form ONB-ester based compound **9**. Treatment with hydrazine hydrate under reflux conditions led to the formation of hydrazine intermediate **10** (for further details, see ESI†). The hydrazine derivative **10,** upon coupling with 4-trifluoromethyl benzaldehyde **7a,** furnished the protransporter **1a** in excellent yield. The sulfide-responsive protransporter **1b** was synthesized using a different procedure due to incompatibility with the above method. Accordingly, compound **5** was reacted with 1-azido-4-(bromomethyl)benzene **11** to form azido-ester derivative **12,** which upon hydrolysis led to the formation of acid derivative **13.** This acid derivative was converted to the acid chloride with oxalyl chloride, followed by coupling with ((trifluoromethyl)benzylidene)hydrazine **15,**

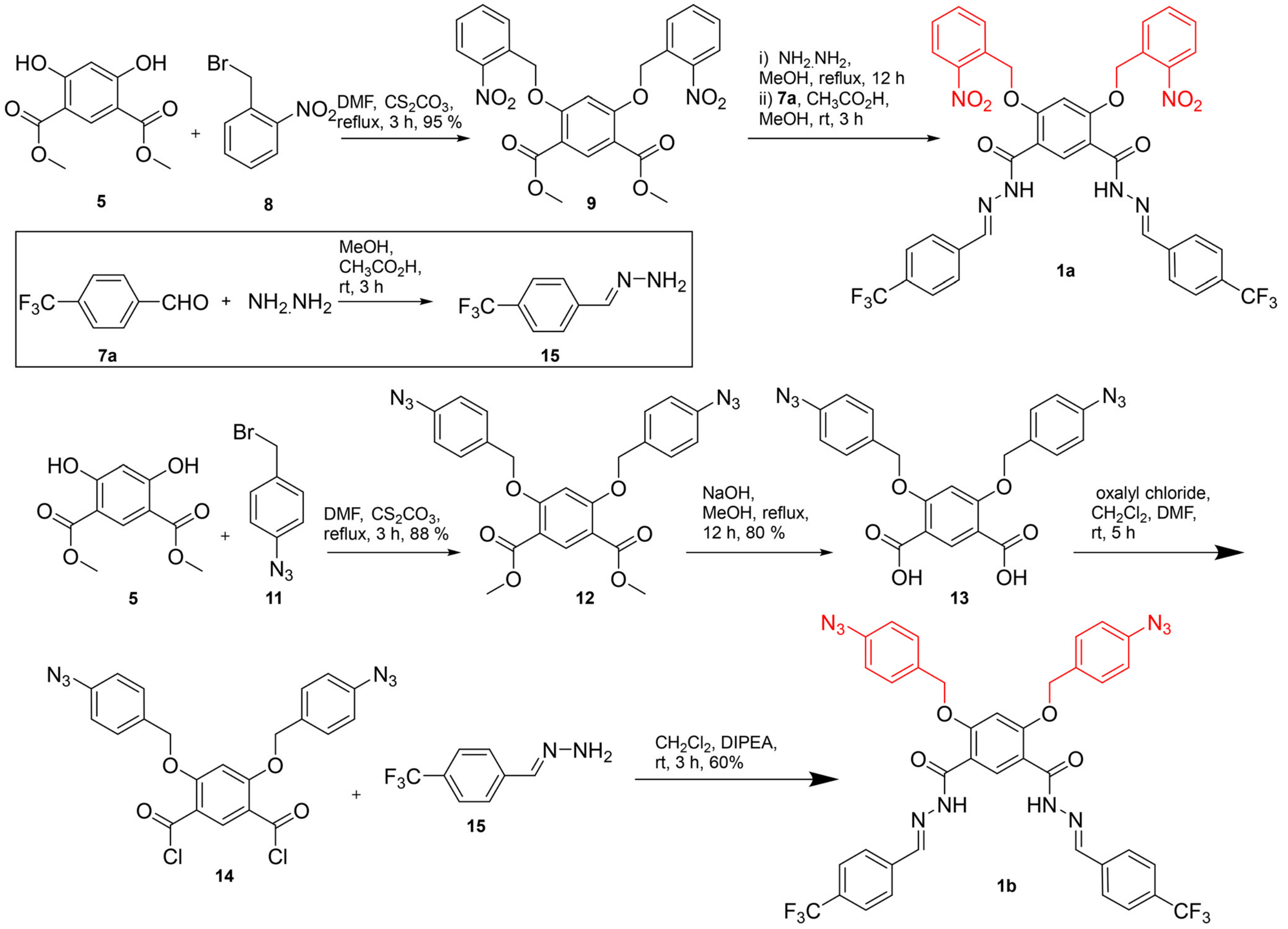

Fig. 5 Chemical synthesis of protransporters **1a** and **1b**.

which itself was prepared by reacting 4-trifluoromethylbenzaldehyde **7a** with hydrazine hydrate, to afford protransporter **1b** in good yield.

Following the synthesis of the pro-transporters, NMR chloride anion binding studies were performed on these caged derivatives. Both **1a** and **1b** displayed very weak anion binding with association constant values of 7 M^{-1} ± 1% for **1a** and 9 M^{-1} ± 2% for **1b**, respectively (Fig. 6C, S44–S47†). This demonstrates that hydrazone protons are locked through six-membered intramolecular hydrogen bonding which makes them unavailable for anion binding. Single crystal X-ray diffraction studies of **1a** confirmed this hypothesis, revealing six-membered intramolecular hydrogen bonding interactions between the hydrazone protons with cage-functionalized attached oxygen atoms (Fig. 6A).

Stimuli-responsive activation studies on **1a** and **1b** were initially performed in solution phase experiments. For **1a**, a solution of the pro-transporter in DMSO-d_6 was subjected to photoirradiation using a 405 nm LED and analysed by ^1H NMR experiments (Fig. S56†). For **1b**, a solution of the pro-transporter in DMF was subjected to sodium hydrosulfide (NaSH, 20 eq.) as the H_2S donor and subjected to HPLC analysis (Fig. S57†). In each case, efficient decaging to generate **1** was observed. With evidence of efficient activation of pro-transporters **1a** and **1b** with light and H_2S in hand, the triggered off-on activation of ion transport was subsequently evaluated using lucigenin-containing LUVs in buffered $NaNO_3$. Pro-transporters **1a** and **1b** were added in an aliquot of DMF (final concentration of 0.30 mol% with respect to lipid), followed by an external chloride pulse. No significant changes were observed in the lucigenin fluorescence, indicating that the pro-transporters are inactive at this concentration, thus achieving an effective off state. Pro-transporter **1a** in buffer solution in a cuvette was then subjected to 405 nm light, before adding LUVs and initiating ion transport by addition of a chloride pulse. Photo-activation of **1a** (0.30 mol%) using a 1 W 405 nm LED resulted in efficient activation, achieving comparable activity to a sample of **1** after 150 s of irradiation, indicative of near quantitative decaging under these conditions (Fig. 7A). For **1b**, a sample in DMF (57 μM, 2.0 mL) was subjected to 10 eq. NaSH for different time intervals (10–40 min), and then aliquots (20 μL) of this solution were added to the cuvette containing the nitrate buffer and LUVs (final concentration of **1b** = 0.30 mol%). Addition of NaSH

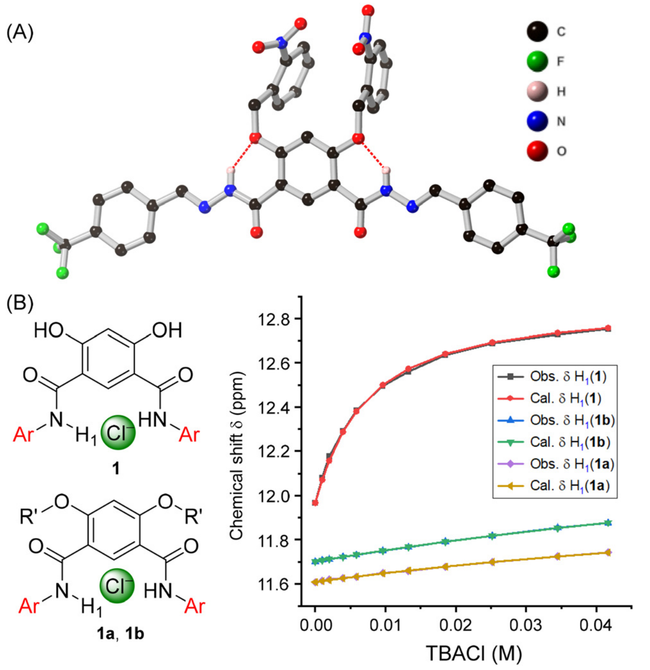

Fig. 6 (A) Molecular structure of pro-transporters **1a** from single crystal X-ray diffraction studies (selected hydrogen atoms and water of crystallisation omitted for clarity). (B) The plot of chemical shift (*δ*) of H_1 proton *vs.* concentration of TBACl added, fitted to 1 : 1 binding model of BindFit v0.5 for active transporters **1** and caged-protransporters **1a** and **1b**, respectively.

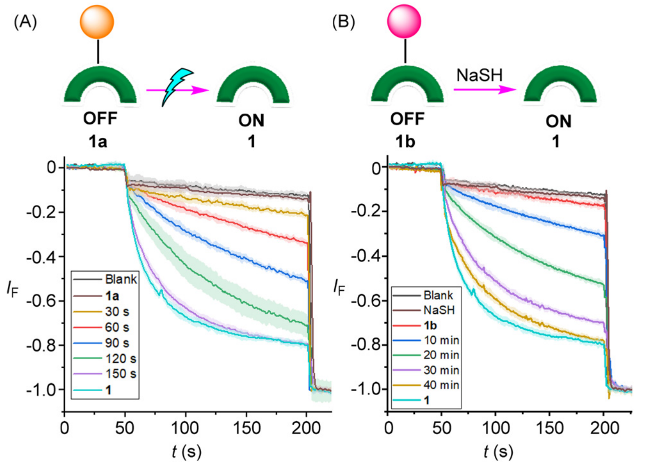

Fig. 7 Ion transport activities across POPC-LUVs ⊃ lucigenin, by (A) photo-irradiating **1a** at 405 nm light using an LED (1 W), and (B) treating **1b** with NaSH (10 eq.) for different time intervals (10–40 min).

generated comparable transport activity to a sample of **1** (Fig. 7B). These results demonstrate that by utilising acylhydrazones within the hydrogen bonding switchable framework, excellent OFF–ON transport activation profiles can be achieved, whilst also enhancing overall transport activity in comparison to the previously reported amide-based system **5′**.

Computational analysis

To further understand the influence of H-bond (HB) interactions and preorganisation on chloride binding, we studied the best-performing transporter, **1**, and its methylated analogue, **1m**, using density functional theory (DFT) calculations.[34–38]

An extensive conformational search confirmed that the minimal energy states **1** and **1m** feature well defined O–H–O and O–H–N hydrogen bonding, respectively, as evidenced by second order perturbation NBO analysis (E^2, Fig. 8A).[39] As expected, based on the enhanced hydrogen bond donor ability of the more electronegative oxygen, the O–H–O HB in **1** are significantly stronger (80 kcal mol^{-1}) than the O–H–N HB in **1m** (20 kcal mol^{-1}, see Fig. S63† for detailed analysis). Moreover, the shorter C═O bond in 1, compared to the C–N bond in **1m**, results in hydrogen bonds that are 0.1–0.2 Å shorter for the intramolecular O–H–O HB in **1** compared to the O–H–N HB in **1m** (Fig. S64–66†).

Chloride binding is favourable in **1** (−2.5 kcal mol^{-1}, in agreement to that determined experimentally by titration: −3.0 kcal mol^{-1}), but endergonic in **1m** (+2.1 kcal mol^{-1}). This can be understood by comparing the change in HB interactions upon binding. While both receptors bind chloride with similar strength (52 *vs.* 49 kcal mol^{-1} from NBO analysis),

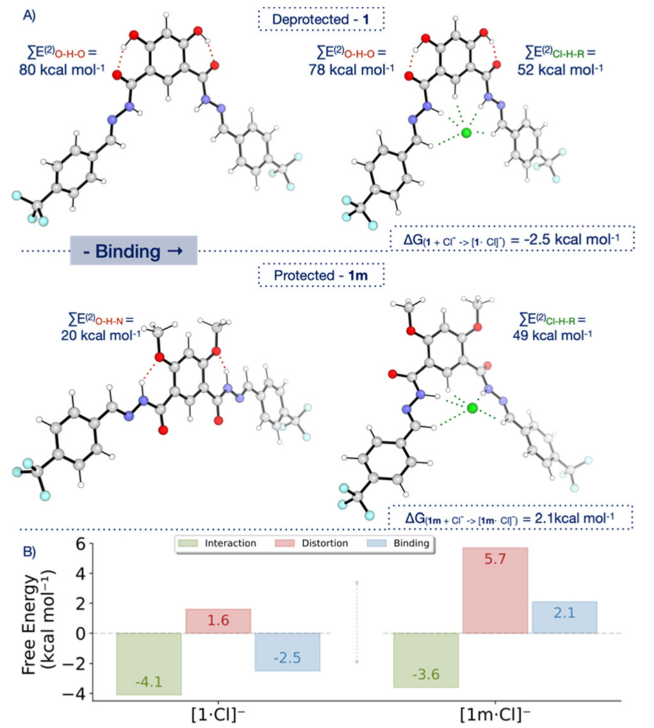

Fig. 8 (A) Summary of DFT optimised structures of protected and deprotected variants of compound **1** with key features highlighted: sums of relevant second order perturbation energies between atoms *X*–*Y*–*Z*, $\sum E^{(2)}_{X-Y-Z}$, as well as chloride binding energies, of geometries calculated at the CPCM(DMSO)-É·B97X-D3/def2-QZVP//CPCM(DMSO)-É·B97X-D3/def2-SVP level. (B) Distortion–interaction analysis of the binding of Cl$^-$ and DMSO to **1** and Cl$^-$ to **1m**.

their intramolecular HBs are significantly different. In **1** the O–H–O HB remains almost intact upon chloride binding (78 *vs.* 80 kcal mol^{-1}), while in **1m** the O–H–N HB is completely broken. Moreover, **1m** shows a significant conformational change upon chloride binding, evidenced by a heavy-atom Root Mean Square Deviation (RMSD) between unbound and bound states of 3.7 Å, which contrast with the small RMSD (0.47 Å) observed for **1** (Fig. S64–66†). To quantify the energetic cost of this conformational change we performed distortion–interaction analysis, which partitions Δ*G* into distortion (energy required to distort the geometry for binding) and interaction (accounting for interactions between host and guest upon binding, Fig. 8B).[40] This analysis confirms that differences in Δ*G* arise almost completely from the greater distortion for **1m** compared to 1 to bind chloride (5.7 *vs.* 1.6 kcal mol^{-1} for 1), while the interaction component is similar (−4.1 and −3.6 kcal mol^{-1} for **1** and **1m**, respectively).

We also explored the role of DMSO solvent coordinating to the transporters, using both DFT and molecular dynamics (MD) simulations. DFT calculations suggest binding of a single DMSO molecule to **1** to be slightly unfavourable but thermally accessible (Δ*G* = 0.8 kcal mol^{-1}, Table S3, and Fig. S65†). A simple Boltzmann weighting gives this [**1**·DMSO] complex in a 1 : 4 ratio to the unbound **1**, but both the small difference in energy and the large concentration of the DMSO solvent suggested that this state would be populated under experimental conditions.

Indeed, unbiased MD simulations of **1** in explicit DMSO solvent confirmed a stable coordination of DMSO to the binding site. Moreover, it showed that the intramolecular O–H–O remains stable during the simulation time (Fig. S69†). To quantify the energy associated with chloride binding in explicit DMSO, we performed both Umbrella Sampling MD (US/MD) and Free Energy Perturbation (FEP) MD simulations (Fig. 9 and Table S4, for further details see ESI†).[41–43]

For US/MD simulations we used the distance between chloride and the centre of mass (CoM) of the central atoms of the binding motif as the pulling coordinate to generate 12 windows spaced 1 Å apart (sampled 3 × 100 ns each using different initial velocities in the NPT ensemble). The resultant free energy profile shows two binding modes of chloride to **1**. Minimum **I** (Δ*G* = −4.3 ± 0.5 kcal mol^{-1}) corresponds to the structure with chloride bound to both hydrazides of 1, similar to the DFT optimised structures. Minimum II (Δ*G* = −2.3 ± 0.5 kcal mol^{-1}) was observed during the dissociation of chloride, where it is bound to one of the hydrazide units as well as the neighbouring phenol, which disrupts the intramolecular O–H–O interaction. These minima are connected by a TS where one of the hydrazide units begins to interact with a DMSO molecule ($\Delta G^{\ddagger}_{\text{Cl}^{-}\ \text{dissociation}}$ = 5.2 ± 0.5 kcal mol^{-1}). Complete dissociation of chloride from **1** leads to re-formation of the O–H–O hydrogen bond and bonding of DMSO by both hydrazides (DMSO bound, Δ*G* = 0 ± 0.2 kcal mol^{-1}). The computed binding energy (−4.3 ± 0.5 kcal mol^{-1}) is higher to the one computed by DFT, possibly due to hysteresis in umbrella sampling. To compute the binding energy in explicit solvent with a more accurate method, we performed FEP simulations, where we found the binding energy to be within error of the experimental value (−3.1 ± 1.1 kcal mol^{-1}), building confidence in the parameters used in the MD simulations, as well as their results.

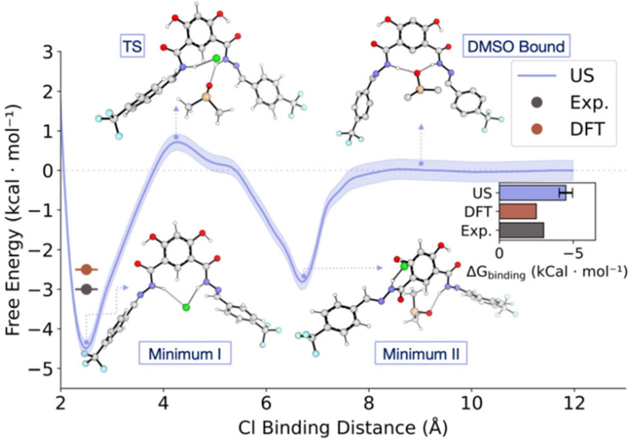

Fig. 9 US/MD energy profile of chloride binding in explicit DMSO. Free energy is reported relative to the chloride-unbound state at a distance of 12 Å to the binding site, defined as the centre of mass (CoM) of the central atoms of the binding motif. This coordinate was used to generate 12 windows spaced 1 Å apart, with a 2000 kJ mol^{-1} nm^{-2} restraint; each window was sampled for 3 × 100 ns in the NPT ensemble, with the first 10% excluded from the analysis. The shaded areas indicating uncertainty from bootstrapping analysis. The bar plot insert compares the binding energies with DFT and experimental values from titration experiments calculated as $-RT\ln(K)$.

III. Conclusion

In conclusion, we have developed stimuli-responsive anion transporters utilizing the dynamic hydrogen bonding interactions of 4,6-dihydroxyisophthalohydrazone anionophores, displaying enhanced activity over previously reported amide-based derivatives. Caging of hydroxyl groups for the most active anionophore **1** with moieties that are responsive to light and H_2S locks the hydrazone protons through six-membered intramolecular hydrogen bonding, rendering them unavailable for anion binding and hence for anion transport. This was confirmed by solid state X-ray crystallographic studies and further validated by NMR binding experiments. Decaging with light and H_2S reverses the hydrogen bonding pattern to switch on anion binding and transport, with efficient off-on activation profiles. DFT calculations highlighted the energetic origins of this incredibly effective switching between an active and an inactive transporter. By using a model truncated system, and including explicit solvent, agreement with experimental binding energies was also obtained, and the inclusion of explicit solvent was validated using molecular dynamics. These results demonstrate the generality of using intra-molecular hydrogen bond switches for developing highly active, stimuli-responsive anionophores, including demonstrating the enhanced activity of systems employing arylhydrazone motifs compared to analogous amide hydrogen bond donors. We anticipate that this methodology should be amenable to integration of any stimuli-cleavable protecting group, such as those already optimised for drug delivery triggered by biological stimuli, providing a platform for future development of targeted therapeutics.

Author contributions

M.J.L. conceived the project and directed the experimental studies. M.A. performed the synthesis and characterization of the compounds, as well as the anion binding and transport studies and stimuli-responsive investigations. M.F. and F.D. performed the theoretical studies. H.T. and A.L.T. performed the crystallographic studies. M.A. and M.F. wrote the first draft of the manuscript, which was edited by all authors.

Data availability

The data supporting this article have been included as part of the ESI.†

Conflicts of interest

There are no conflicts to declare.

Acknowledgements

M. A. and M. J. L. acknowledge the Leverhulme Trust (RPG-2020-130) for financial support. M. F. thanks the Centre for Doctoral Training in Synthesis for Biology and Medicine for a studentship, generously supported by GlaxoSmithKline, MSD, Syngenta and Vertex. H. M. T acknowledges the Clarendon Fund and Oxford Australia Scholarships Fund for a post-graduate research scholarship. M. J. L. is a Royal Society University Research Fellow.

References

1 G. Nagel, D. Ollig, M. Fuhrmann, S. Kateriya, A. M. Musti, E. Bamberg and P. Hegemann, *Science*, 2002, **296**, 2395.
2 W. A. Catterall, *Annu. Rev. Biochem.*, 1995, **64**, 493–531.
3 M. Jaiteh, A. Taly and J. Hénin, *PLoS One*, 2016, **11**, e0151934.
4 J. Y. Choi, D. Muallem, K. Kiselyov, M. G. Lee, P. J. Thomas and S. Muallem, *Nature*, 2001, **410**, 94–97.
5 S. B. H. Hladky and D. A. Ion, Movement in GramicidinChannels, in *Current Topics in Membranes and Transport*, ed. F. Bronner, Academic Press, New York, 1984, Vol. 21, pp. 327–372.
6 R. D. Vaughan-Jones, K. W. Spitzer and P. Swietach, *J. Mol. Cell. Cardiol.*, 2009, **46**, 318–331.
7 V. Soto-Cerrato, P. Manuel-Manresa, E. Hernando, S. Calabuig-Fariñas, A. Martínez-Romero, V. Fernández-Dueñas, K. Sahlholm, T. Knöpfel, M. García-Valverde, A. M. Rodilla, E. Jantus-Lewintre, R. Farràs, F. Ciruela, R. Pérez-Tomás and R. Quesada, *J. Am. Chem. Soc.*, 2015, **137**, 15892–15898.
8 S.-K. Ko, S. K. Kim, A. Share, V. M. Lynch, J. Park, W. Namkung, W. Van Rossom, N. Busschaert, P. A. Gale, J. L. Sessler and I. Shin, *Nat. Chem.*, 2014, **6**, 885–892.
9 N. Busschaert, M. Wenzel, M. E. Light, P. Iglesias-Hernández, R. Pérez-Tomás and P. A. Gale, *J. Am. Chem. Soc.*, 2011, **133**, 14136–14148.
10 T. Saha, A. Gautam, A. Mukherjee, M. Lahiri and P. Talukdar, *J. Am. Chem. Soc.*, 2016, **138**, 16443–16451.
11 E. N. W. Howe, N. Busschaert, X. Wu, S. N. Berry, J. Ho, M. E. Light, D. D. Czech, H. A. Klein, J. A. Kitchen and P. A. Gale, *J. Am. Chem. Soc.*, 2016, **138**, 8301–8308.
12 A. Roy, O. Biswas and P. Talukdar, *Chem. Commun.*, 2017, **53**, 3122–3125.
13 Y. R. Choi, G. C. Kim, H.-G. Jeon, J. Park, W. Namkung and K.-S. Jeong, *Chem. Commun.*, 2014, **50**, 15305–15308.
14 E. B. Park and K.-S. Jeong, *Chem. Commun.*, 2015, **51**, 9197–9200.
15 M. M. Tedesco, B. Ghebremariam, N. Sakai and S. Matile, *Angew. Chem., Int. Ed.*, 1999, **38**, 540–543.
16 G. A. Woolley, M. K. Kapral and C. M. Deber, *FEBS Lett.*, 1987, **224**, 337–342.
17 N. Akhtar, N. Pradhan, A. Saha, V. Kumar, O. Biswas, S. Dey, M. Shah, S. Kumar and D. Manna, *Chem. Commun.*, 2019, **55**, 8482–8485.
18 A. Docker, T. G. Johnson, H. Kuhn, Z. Zhang and M. J. Langton, *J. Am. Chem. Soc.*, 2023, **145**, 2661–2668.
19 X. Wu, J. R. Small, A. Cataldo, A. M. Withecombe, P. Turner and P. A. Gale, *Angew. Chem., Int. Ed.*, 2019, **58**, 15142–15147.
20 M. Ahmad, S. Chattopadhayay, D. Mondal, T. Vijayakanth and P. Talukdar, *Org. Lett.*, 2021, **23**, 7319–7324.
21 M. Ahmad, D. Mondal, N. J. Roy, T. Vijayakanth and P. Talukdar, *ChemPhotoChem*, 2022, e202200002.
22 M. Ahmad, S. Metya, A. Das and P. Talukdar, *Chem. – Eur. J.*, 2020, **26**, 8703–8708.
23 A. Kerckhoffs, Z. Bo, S. E. Penty, F. Duarte and M. J. Langton, *Org. Biomol. Chem.*, 2021, **19**, 9058–9067.
24 A. Kerckhoffs and M. J. Langton, *Chem. Sci.*, 2020, **11**, 6325–6331.
25 T. G. Johnson, A. Sadeghi-Kelishadi and M. J. Langton, *J. Am. Chem. Soc.*, 2022, **144**, 10455–10461.
26 C. Wang, S. Wang, H. Yang, Y. Xiang, X. Wang, C. Bao, L. Zhu, H. Tian and D. H. Qu, *Angew. Chem., Int. Ed.*, 2021, **60**, 14836–14840.
27 S. J. Wezenberg, L.-J. Chen, J. E. Bos, B. L. Feringa, E. N. W. Howe, X. Wu, M. A. Siegler and P. A. Gale, *J. Am. Chem. Soc.*, 2022, **144**, 331–338.
28 M. Ahmad, N. J. Roy, A. Singh, D. Mondal, A. Mondal, T. Vijayakanth, M. Lahiri and P. Talukdar, *Chem. Sci.*, 2023, **14**, 8897–8904.

29 S. B. Salunke, J. A. Malla and P. Talukdar, *Angew. Chem., Int. Ed.*, 2019, **58**, 5354–5358.

30 C. Bao, M. Ma, F. Meng, Q. Lin and L. Zhu, *New J. Chem.*, 2015, **39**, 6297–6302.

31 L. E. Bickerton and M. J. Langton, *Chem. Sci.*, 2022, **13**, 9531–9536.

32 Q. Zhong, Y. Cao, X. Xie, Y. Wu, Z. Chen, Q. Zhang, C. Jia, Z. Wu, P. Xin, X. Yan, Z. Zeng and C. Ren, *Angew. Chem., Int. Ed.*, 2024, **63**, e202314666.

33 M. Ahmad, T. G. Johnson, M. Flerin, F. Duarte and M. J. Langton, *Angew. Chem., Int. Ed.*, 2024, **63**, e202403314.

34 F. Neese, *Wiley Interdiscip. Rev.: Comput. Mol. Sci.*, 2022, **12**, e1606.

35 J.-D. Chai and M. Head-Gordon, *Phys. Chem. Chem. Phys.*, 2008, **10**, 6615–6620.

36 F. Weigend and R. Ahlrichs, *Phys. Chem. Chem. Phys.*, 2005, **7**, 3297–3305.

37 V. Barone and M. Cossi, *J. Phys. Chem. A*, 1998, **102**, 1995–2001.

38 E. D. Glendening, C. R. Landis and F. Weinhold, *J. Comput. Chem.*, 2013, **34**, 1429–1437.

39 S. Grimme, *J. Chem. Theory Comput.*, 2019, **15**, 2847–2862.

40 F. M. Bickelhaupt and K. N. Houk, *Angew. Chem., Int. Ed.*, 2017, **56**, 10070–10086.

41 A. Lindahl, *Hess and van der Spoel, GROMACS 2021.3 Source code (version 2021.3)*, Zenodo, 2021.

42 J. S. Hub, B. L. de Groot and D. van der Spoel, *J. Chem. Theory Comput.*, 2010, **6**, 3713–3720.

43 C. H. Bennett, *J. Comput. Phys.*, 1976, **22**, 245–268.